The structure of human CD23 and its interactions with IgE and CD21

Richard G. Hibbert,[1] Peter Teriete,[1] Gabrielle J. Grundy,[2] Rebecca L. Beavil,[2] Rajko Reljić,[2] V. Michael Holers,[3,4] Jonathan P. Hannan,[3] Brian J. Sutton,[2] Hannah J. Gould,[2] and James M. McDonnell[1]

[1]Laboratory of Molecular Biophysics, Department of Biochemistry, University of Oxford, Oxford OX1 3QU, England, UK
[2]Randall Division of Cell and Molecular Biophysics, King's College London, London SE1 1UL, England, UK
[3]Department of Medicine and [4]Department of Immunology, Health Science Center, University of Colorado, Denver, CO 80262

The low-affinity immunoglobulin E (IgE) receptor, CD23 (FcεRII), binds both IgE and CD21 and, through these interactions, regulates the synthesis of IgE, the antibody isotype that mediates the allergic response. We have determined the three-dimensional structure of the C-type lectin domain of CD23 in solution by nuclear magnetic resonance spectroscopy. An analysis of concentration-dependent chemical shift perturbations have allowed us to identify the residues engaged in self-association to the trimeric state, whereas ligand-induced changes have defined the binding sites for IgE and CD21. The results further reveal that CD23 can bind both ligands simultaneously. Despite the C-type lectin domain structure, none of the interactions require calcium. We also find that IgE and CD23 can interact to form high molecular mass multimeric complexes. The interactions that we have described provide a solution to the paradox that CD23 is involved in both up- and down-regulation of IgE and provide a structural basis for the development of inhibitors of allergic disease.

CORRESPONDENCE
James M. McDonnell:
jim@biop.ox.ac.uk

Abbreviations used: CTLD, C-type lectin-like domain; D, dalton; MBP, mannose-binding protein; NMR, nuclear magnetic resonance; NOE, nuclear overhauser effect; ppm, parts per million, r.m.s., root mean squared.

IgE binds to its effector cells through either FcεRI, the high-affinity receptor, or CD23 (FcεRII), the low-affinity receptor. The former mediates the IgE effector functions with mast cells and basophils in type I immediate hypersensitivity. CD23 has multiple functions that are controlled by a range of different ligands. These include IgE (both in its secreted form and on membranes of committed B cells), CD21 (also known as complement receptor 2), CD18/CD11b and CD18/CD11c (complement receptors 3 and 4, respectively), and the vitronectin receptor (1). The interactions with IgE and CD21 are pivotal in IgE regulation (2). Paradoxically, CD23 engages in both the up- and down-regulation of IgE synthesis, thereby constituting a two-way switch in IgE homeostasis (reviewed in reference 1).

CD23 is a 45-kD type II membrane protein expressed in various cell types, including B cells. It is unique among Fc receptors in its homology to C-type (calcium-dependent) lectins (1) and is also closely homologous, and genetically linked on human chromosome 19, to DC-SIGN (3). IgE and CD21 are known to bind to this lectin domain (4). Two CD23 lectin domains can bind to the Cε3 domains in IgE (5). CD21 comprises a tandem array of 15–16 short consensus repeat domains; CD23 binds to domains 1–2 (D1-2) and domains 5–8 (D5-8) via protein–protein and protein–carbohydrate interactions, respectively (6).

The structures of the CD23 ligands, IgE Fc (7) (as well as the Cε3-4 subfragment [8]), and the two NH_2-terminal short consensus repeat domains of CD21(D1-2) (9) are known from X-ray crystallography. In contrast, that of the CD23 lectin domain has only been inferred by modelling, based on available sequence homologies (10). We have used nuclear magnetic resonance (NMR) to determine the three-dimensional structure of the lectin domain and to locate the residues involved in IgE and CD21 binding. We have also searched for the interactions of the lectin domain with calcium and a set of possible mono/disaccharide ligands to evaluate its lectin function.

Like DC-SIGN and several other C-type lectins, CD23 self-associates through its extracellular sequence by the formation of an α-helical coiled-coil "stalk." In the membrane of B cells, CD23 forms trimers with the three

G.J. Grundy's present address is Laboratory of Molecular Biology, National Institute of Diabetes and Digestive and Kidney Diseases, National Institutes of Health, Bethesda, MD 20892.

The online version of this article contains supplemental material.

The Journal of Experimental Medicine

lectin domains held together at the end of the 15-nm stalk (11). The stalk is susceptible to proteolytic cleavage (12), generating fragments with differing trimerization propensities depending on the length of the residual stalk. The dust mite protease Der p I cleaves CD23 close to the lectin domain, and the resulting monomeric CD23 may be a factor in the high allergenicity of dust mites (13). We have determined the structure of a recombinant version of the Der p I fragment of CD23 (derCD23) by NMR spectroscopy, as well as the location of the IgE and CD21 binding sites. For comparison, we also generated a recombinant soluble CD23 fragment containing the entire extracellular sequence (exCD23).

The opposing activities of CD23 in IgE regulation are thought to be properties of the soluble and membrane forms. Soluble CD23 enhances IgE synthesis on binding to CD21 (2). When IgE binds to membrane CD23, further IgE synthesis is suppressed; in CD23-deficient mice, the level of circulating IgE is increased by orders of magnitude (14). The balance between the two forms of CD23 may accordingly be expected to regulate the level of IgE synthesis.

CD23 fragments are found in the circulation of normal human subjects. Elevated concentrations of circulating soluble fragments are commonly associated with inflammatory or lymphoproliferative diseases, such as rheumatoid arthritis, asthma, and chronic lymphoblastic leukemia, also known as CLL (15–17). It has been shown that antibodies to CD23 alleviate all three conditions, and an anti-CD23 antibody, IDEC-152, is in clinical trials for asthma (16) and CLL (17). Structural information on CD23 and its interactions is needed if the mechanisms of IgE homeostasis are to be understood and agents for intervening in this process developed.

RESULTS

derCD23 interacts with IgE and CD21

We have used surface plasmon resonance to characterize the interaction between derCD23 and the two protein ligands, IgE and CD21, involved in IgE regulation, determining equilibrium and rate constants for the Fc fragment of IgE (domains Cε2-4) and the D1-2 fragment of human CD21.

For the interaction between Cε2-4 and derCD23, we observed a marked change in affinity and off rates depending on the immobilization density of derCD23. At low density, Cε2-4 and CD21(D1-2) both show fast-on/-off kinetics with a resulting $K_D = 1.3 \pm 0.3$ and $0.87 \pm 0.09 \times 10^{-6}$ M, respectively (Fig. 1, A and B). At a higher immobilization density of derCD23 the rates of dissociation of Cε2-4 are markedly reduced (Fig. 1 D). Cε2-4 is a dimer, and the presence of two copies of the Cε3 domain may therefore explain this effect; the dimer has the potential to make a bivalent interaction and the observed affinity differences are then caused by cooperative binding. The monovalent CD21(D1-2) construct showed no change in apparent affinity at higher derCD23 densities (Fig. 1 C).

When Cε2-4 is the immobilized component, binding of derCD23 (Fig. 1 E), which is monomeric under these conditions as shown by sedimentation equilibrium (molecular mass = 18,086 ± 350 dalton [D]; unpublished data), gives similar values to Cε2-4/derCD23 (Fig. 1 B). In contrast, the binding of exCD23, with the complete extracellular sequence, shows a considerably higher affinity, with a markedly slower off rate (Fig. 1 F). In fact, these binding curves of exCD23 with Cε2-4 show two components with different affinities ($K_D = 1.1 \pm 0.2 \times 10^{-6}$ M and $3.9 \pm 0.6 \times 10^{-8}$ M) and interaction kinetics. This effect is clearly reflected in the dissociation kinetics (Fig. 1 F; one minor component with a rate constant of 4×10^{-2} s^{-1} and a major component with an off-rate constant of 5×10^{-4} s^{-1}). Because exCD23 is also monomeric in solution under these conditions, as de-

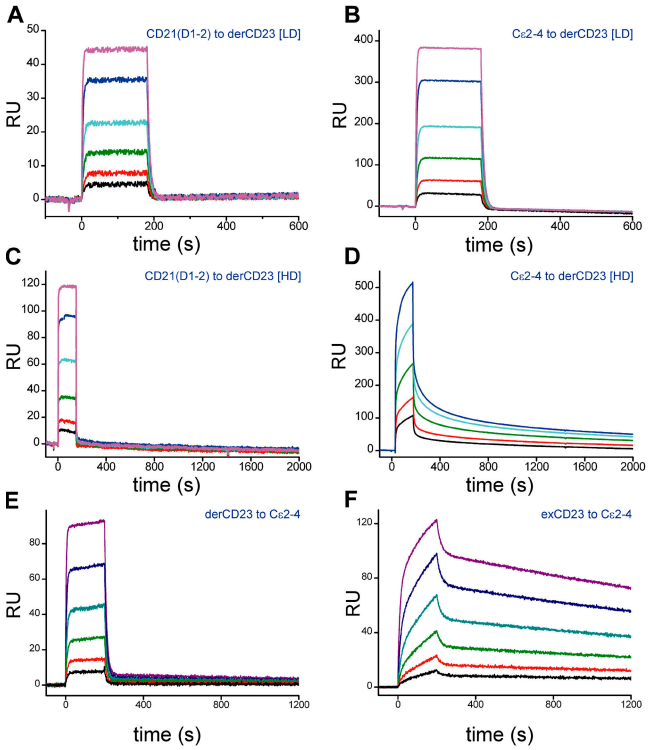

Figure 1. Surface plasmon resonance analysis of CD23 interactions with CD21 and IgE. The binding of CD21(D1-2) (A and C) and IgE Cε2-4 (B and D) to immobilized derCD23 was determined over a range of ligand concentrations: 62.5 (black), 125 (red), 250 (green), 500 (cyan), 1,000 (blue), and 2,000 nM (purple). Binding to CD23 was tested at a low ligand density (LD; panels A and B) and at a high ligand density (HD; panels C and D). The reverse orientation, binding derCD23 and exCD23 to immobilized Cε2-4 (E and F), was also characterized for the same concentration range. Representative sensorgrams are shown here. The K_D value for the monomeric interactions between derCD23 and CD21(D1-2) (A and C) is $8.7 \pm 0.9 \times 10^{-7}$ M and for derCD23 to Cε2-4 (B and E) is $1.3 \pm 0.3 \times 10^{-6}$ M. The interaction between exCD23 and Cε2-4 (F) shows a distinct biphasicity, with two binding constants of $1.1 \pm 0.2 \times 10^{-6}$ and $3.9 \pm 0.6 \times 10^{-8}$ M. The interaction between Cε2-4 and the high-density derCD23 surface (D) show complex kinetics that indicate several distinct binding events. It is markedly different from the interaction with the low density derCD23 surface (B), showing much slower dissociation rates.

termined by sedimentation equilibrium (molecular mass = 30,426 ± 908 D; unpublished data), this biphasicity must be caused by formation of dimers or trimers by enhanced self-association of lectin domains as they bind to IgE Fc. Thus, binding of soluble CD23 to IgE Fc promotes oligomerization, provided that there is sufficient stalk, as in exCD23. A weak interaction between CD23 lectin domains is also evident from our NMR studies of derCD23 at elevated concentrations (see derCD23 oligomerization). Upon oligomerization of CD23 in the complex with IgE Fc, it will gain the capacity to bind additional IgE Fc molecules. Indeed, the sedimentation equilibrium profile indicates the formation of a heterogeneous mixture of high molecular mass complexes, which cannot be modeled to determine its size distribution (unpublished data).

The analogy with other members of the C-type lectin superfamily would suggest that the structure and activity of CD23 might be dependent on calcium, and there is some experimental evidence in favor of this inference (18, 19). We performed binding experiments in the presence of 10 mM EDTA after stripping derCD23 of calcium by overnight incubation in EDTA. The binding of IgE Fc showed a small (sevenfold) decrease in affinity (to a K_D of $9.1 \pm 0.9 \times 10^{-6}$ M) due almost entirely to a change in on rate (unpublished data). This is consistent with the expectation that the calcium affects the conformation of certain loops, based on observations of other C-type lectins, but calcium is not involved directly in binding. The affinity of the CD21(D1-2) interaction was unaffected by the removal of calcium.

Table I. Summary of restraints and structural statistics[a]

Component	Quantity
Restraints	
NOEs	
Intraresidue	973
Sequential	421
Medium range ($i < 5$)	213
Long range	572
Total NOEs	2179
Dihedral Angles (ϕ and ψ)	96
Hydrogen bonds	30
Total number of restraints	2335
Number of violations	
Distance restraints (>0.3 Å)	0
Dihedral angle restraints (>5°)	0
Precision[b,c]	
Backbone heavy atoms (Å)	0.267
All heavy atoms (Å)	0.854
Structure quality	
Residues in most favored regions	65.4%
Residues in additionally allowed regions	27.7%
Residues in generously allowed regions	5.2%
Residues in disallowed regions	1.7%

[a]The three-dimensional coordinate file for the protein is available from the Protein Data Bank under accession no. 1T8D.
[b]Values reported are the average values greater than the 20 lowest energy structures.
[c]The average r.m.s. deviation for the coordinates set was calculated by superimposing each of the 20 structures onto the lowest energy structure. The superposition was over backbone and heavy atoms of residues 166–169, 172–178, 183–193,196–198, 204–213, 217–225, 230–234, 158–162, 266–271, and 278–285.

The structure of CD23

The three-dimensional structure of derCD23 was solved by heteronuclear NMR spectroscopy, and its interactions with its ligands were examined. Assignment of backbone and side-chain resonances were performed by CBCA- and nuclear overhauser effect (NOE)–based assignment strategies; trosy-based pulse sequences were used to improve the efficiency of the triple resonance experiments (20). Additional data were collected to characterize derCD23 dynamics and hydrodynamics. Analysis of dynamics from ^{15}N relaxation gives a direct measure of backbone flexibility. The derCD23 lectin domain is generally structurally rigid, with highly flexible NH_2 and COOH termini and three internal loops (α2-β4, β4-β5, and β5-β6) showing some degree of flexibility. Five amino acids from a central loop (β5-β6) could not be assigned; residues flanking this loop show increased transverse relaxation rates, suggesting that this region experiences motions on the ms-μs time scale and that loss of peaks is probably caused by line broadening (NMR relaxation data are shown in Fig. S1, available at http://www.jem.org/cgi/content/full/jem.20050811/DC1).

The structure of derCD23 was based on >2,300 NMR-derived structural constraints, including >2,100 structurally relevant NOEs, 96 dihedral angle constraints from the program TALOS (see Materials and methods) (21), and 30 hydrogen bonds, implied by hydrogen–deuterium exchange experiments and local secondary structure. A summary of restraints used is shown in Table I. The average density of structural constraints was ~25 per residue over the secondary structure elements of the protein.

The three-dimensional structure of derCD23 consists of two roughly orthogonal α helices and eight β strands forming two antiparallel β sheets. Four disulphide bonds contribute to the tertiary structure, whereas seven tryptophan residues and other conserved side chains form a hydrophobic core within the domain. The topology is that of a C-type lectin domain. It shows the greatest sequence and structural homology to the lectin domains of DC-SIGN, the H1 subunit of the asialoglycoprotein receptor, and human lung surfactant protein D, with sequence identities of 36, 35, and 26%, respectively, and root mean squared (r.m.s.) deviations of 2.7–2.8 Å over 118–126 residues. The global r.m.s. deviation for the NMR-derived ensemble of 20 structures is 0.26 Å for backbone atoms and 0.8 Å for heavy atoms in all elements of secondary structure. A bundle of the 20 lowest energy conformers and a ribbon diagram of the derCD23 structure are shown in Fig. 2, A and B, respectively. derCD23 shows a marked polarity in its electrostatic character. The

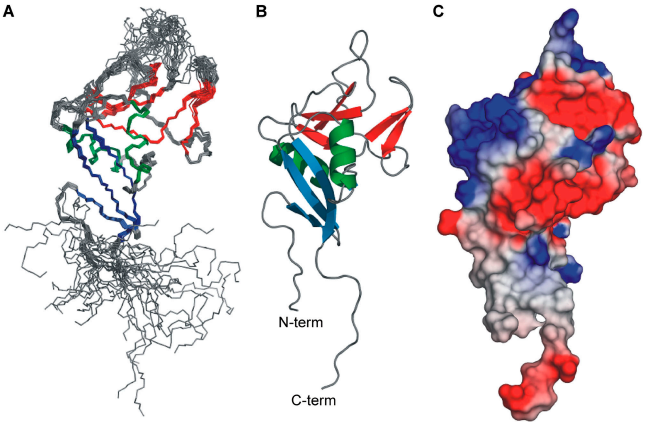

Figure 2. The structure of derCD23. (A) View of the backbone (N, Cα, C′) of 20 superimposed NMR-derived structures of derCD23. (B) A ribbon diagram of the lowest energy conformer of derCD23, with secondary structural elements identified. (C) A surface representation of derCD23 colored according to electrostatic potential and coded such that regions with a potential <-4 k_BT are red, whereas those >4 k_BT are blue. k_B, Boltzmann constant; T, absolute temperature.

surface is highly charged, but the positive and negative charges are found on opposite faces (Fig. 2 C). The highly charged character will affect how CD23 interacts with ligands and appears to be particularly important in self-association.

We observed two distinct conformations for the derCD23 protein (conformations A and B, available from the Protein Data Bank under accession nos. 1T8D and 1T8C, respectively) in an area around the hydrophobic face of α-helix 1. Twenty residues show two sets of peaks in ^{1}H-^{15}N–HSQC spectra. Based on relative peak intensities, the two conformations are roughly equally populated. The relative occupancies of the conformations did not change under a large number of conditions tested, including changes in concentration, temperature, pH, and ionic strength and in several ligand-binding experiments. The two conformations are in slow exchange on the NMR timescale. Each conformer gave rise to a distinct set of NOEs; based on 220 distinct NOEs, independent ensembles of structures were calculated for each conformation. The two conformations differ in the extent of hydrophobic packing between the first β sheet (β1, β2, β3, and β8) and α-helix 1. This results in small changes in overall structure but marked changes in chemical shift for nearby residues because of the change of orientation of three aromatic side chains (Y176, W167, and W280) in this region. Because the biological importance of these two conformers is not clear at present, we will not dwell on them further here, and they will be described in detail elsewhere (unpublished data).

The CD23 calcium binding site and the lectin functions of CD23

X-ray crystallography of related C-type lectin-like domains (CTLDs) has shown one to three calcium binding sites per domain (22), but the calcium and carbohydrate binding properties of CD23 have been difficult to predict. Ca^{2+} site 2 in derCD23 is reasonably well conserved, but the canonical Ca^{2+} site 1 is poorly conserved (23). In other CTLDs, site 2 is directly involved in binding carbohydrates.

We studied the calcium-binding behavior of derCD23 by monitoring the effects of calcium titration on the ^{1}H-^{15}N–HSQC spectrum. derCD23 was expressed and refolded in the presence of 25 mM EDTA, and the EDTA was removed by dialysis. The calcium-free sample was well folded with only very few residues showing substantial chemical shift changes from the calcium-bound sample, in contrast to some other CTLDs that require Ca^{2+} for proper folding (24). Eleven datasets were collected with Ca^{2+} concentrations ranging from 100 μM to 50 mM. Over the course of this titration, seven residues showed large proton chemical shift changes (>0.08 parts per million [ppm]): backbone amides for I221, N225, K229, G230, E231, D270, A271, and D274 and the side-chain amide resonances of N225. Saturation binding curves for each of the eight sites were measured, and all were in good agreement, giving a K_D of 1.80 ± 0.15 mM (Fig. 3, inset). Surprisingly, the observed pattern of chemical shift changes suggests occupancy of Ca^{2+} site 1, but presents no evidence for the occupancy of Ca^{2+} site 2 (Fig. 3).

We also tested the ability of derCD23 to interact with a series of carbohydrate ligands. Individual NMR chemical shift perturbation titrations were performed with galactose, glucose, lactose, mannose, and N-acetylglucosamine to a fi-

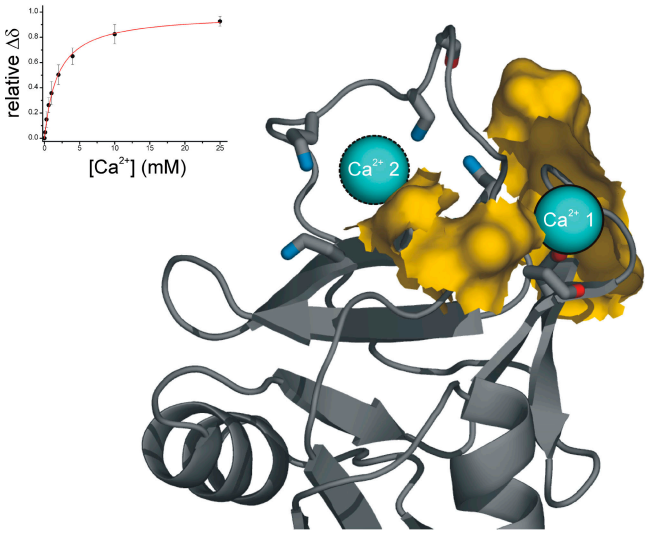

Figure 3. The calcium binding site on CD23. The backbone cartoon of CD23 is shown in gray and the canonical CTLD calcium ions are indicated with blue spheres. Conserved potential chelating atoms are indicated and are colored red for site 1 and blue for site 2. Residues that show large changes in chemical shift ($\Delta\delta_{HN} \geq 0.08$ ppm) on the addition of calcium are mapped onto the protein surface and are indicated in yellow. The inset shows the binding isotherm based on change in chemical shift position; results and standard deviations (K_D of 1.80 ± 0.15 mM) are from the seven residues that show proton chemical shift changes of ≥0.08 ppm. These results suggest the occupancy of Ca^{2+} site 1 only.

nal carbohydrate concentration of 125 mM. Even at the highest concentrations, none of these compounds bound to derCD23. In conjunction with the apparent absence of Ca^{2+} site 2, CD23, if it binds sugars at all, must do so using a different mode from the canonical CTLD carbohydrate recognition mechanism.

The interaction surface of derCD23 for IgE

To investigate the nature of the CD23's interaction with IgE, the Fc fragment of IgE (Cε2-4) was titrated with ^{15}N-labeled derCD23. During the titration, most of the peaks in the trosy-HSQC spectrum disappeared because of line broadening. Only peaks mapping to the COOH terminus of the derCD23 fragment remained visible (unpublished data); the relaxation analysis indicated that these residues have motion independent from the overall tumbling characteristics of the protein. These observations are consistent with the formation of a high-order oligomer of the Cε2-4–derCD23 complex.

To map the ligand binding surfaces of CD23 with IgE, we instead titrated a monomeric Cε3 domain against a ^{15}N-labeled derCD23 sample (Fig. 4 A). It has been reported that the entire CD23 binding site is contained within the Cε3 domain (25). Residues W184, R188, Y189, A190, L198, H202, I221, G222, R224, N225, L226, W234, V235, A271, C273, D274, K276, and A279 in derCD23 exhibited considerable concentration-dependent changes in chemical shifts and line broadening on addition of Cε3. The residues, when mapped onto the derCD23 surface, reveal a continuous interaction surface for Cε3 on the CD23 lectin domain (Fig. 4 C). The complete list of chemical shift changes observed during the Cε3 titration are available in the BioMagResBank database under accession no. 6734.

The interaction surface of derCD23 for CD21

We identified the interaction surface of CD21 on CD23 by titrating unlabeled CD21(D1-2) against ^{15}N-labeled derCD23 (Fig. 4 B). This CD21 construct is identical to the one cocrystallized with C3d (9). Four residues of derCD23 show chemical shift perturbations, all of which are in the COOH-terminal "tail" (residues E294, G295, S296, and E298; Fig. 4 C). Residue S293 was not assigned, whereas the peak for residue A297 lies in a region of considerable overlap in the ^{15}N-HSQC, making it difficult to identify its position unambiguously. Residue A292 does not show a change in chemical shift, and, hence, we infer that the CD21 interaction site comprises the COOH-terminal six residues of this CD23 construct. We note that the full-length CD23 COOH-terminal tail, with an additional 23 residues, may have a higher affinity for CD21 than the derCD23 fragment. Further studies will focus on this and the binding to other domains of CD21 (6).

Despite a high degree of conservation between the lectin head region of human and mouse CD23 (62% over 143 residues), the COOH-terminal region of derCD23 is not conserved between species (2 identities over the 10 COOH-ter-

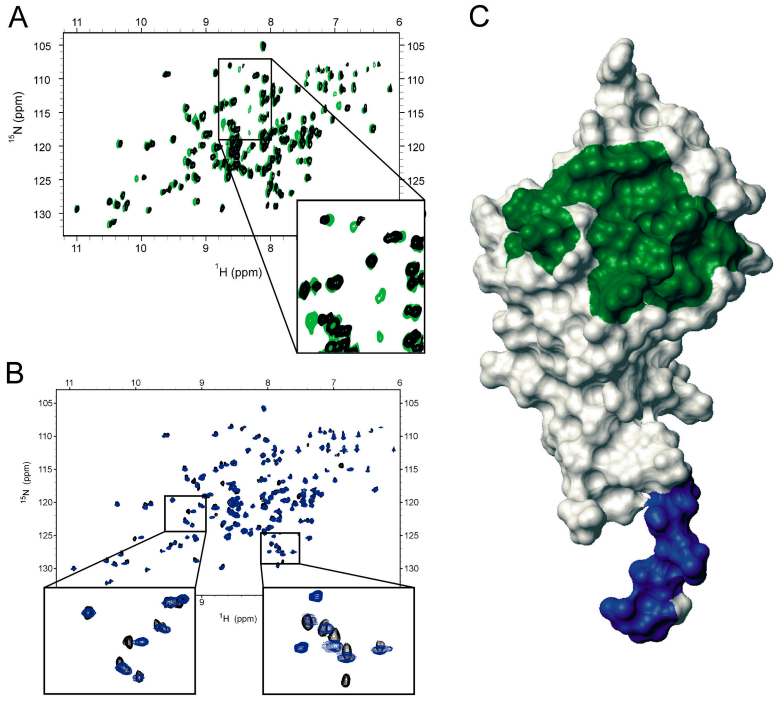

Figure 4. ^{1}H–^{15}N chemical shift perturbation experiments define the interaction surfaces on derCD23 for Cε3 and CD21(D1-2). A small number of residues show chemical shift perturbation on addition of IgE Cε3 or CD21(D1-2). Example spectra illustrating this are shown in (A) and (B), respectively. Insets show expanded views of the indicated areas. (C) Residues that show substantial chemical shift changes are mapped onto the derCD23 surface and are colored green for Cε3 and blue for CD21(D1-2). The orientation of this molecule is identical to that shown in Fig. 2.

minal residues). Thus, the location of the CD21 binding site suggests that this interaction may not occur in the mouse, in agreement with binding studies (Conrad, D.H., personal communication). This helps to explain important differences in IgE regulation between human and murine systems (see below).

The CD23–IgE–CD21 trimolecular complex

The two NMR titration experiments identify independent binding sites for CD21(D1-2) and IgE on CD23. We confirmed the independent nature of the interactions by forming the trimolecular complex (derCD23–Cε3–CD21(D1-2)) through sequential titrations showing additivity of the effects on the spectrum of the separate interactions (unpublished data).

derCD23 oligomerization

At a concentration of 100 μM, derCD23 has an apparent molecular mass of 16.5 kD, but at 1.2 mM of derCD23 a monomer–oligomer equilibrium supervened, with a mass-average molecular mass of ~28 kD, with both values estimated from NMR-based translational diffusion measurements (26). This self-association is accompanied by a change in the chemical shifts of some of the peaks in the HSQC spectrum. These residues (L198, K212, H213, N225, E231, V240, and Y242) map to the two distinct regions with opposite charge characteristics and suggest a possible self-association interaction surface.

On the basis of this postulated interaction surface, we generated a model for the trimer formed by full-length CD23 (Fig. 5). X-ray structures of other C-type lectin trimers have been determined, and the arrangement of the subunits are all similar in mannose-binding protein (MBP), pulmonary surfactant apoproteins D and A, and tetranectin (23). The NMR data predict a different arrangement for the CD23 trimer. MBP, pulmonary surfactant apoproteins D and A, and tetranectin all possess a similar nucleating heptad repeat sequence at the top of the coiled-coil stalk that allows the formation of a largely hydrophobic interface. Although CD23 has strong homology to these proteins in the lectin-like domain, it differs in this interface motif. Furthermore, an MBP-type arrangement for CD23 would result in an electrostatically repulsive interface. The interface predicted from the NMR chemical shifts presents an electrostatically favorable interface and results in completely solvent-exposed interaction sites for IgE and CD21 (Fig. 5).

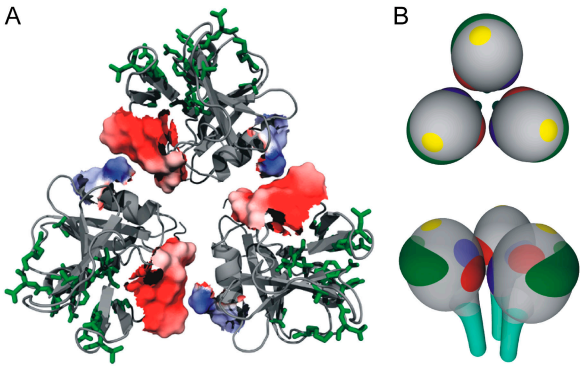

Figure 5. The CD23 trimer and the architecture of ligand interaction sites. (A) An overhead view of the postulated CD23 trimer is shown. For each monomer, a backbone ribbon cartoon is shown in gray, and residues that show concentration-dependent chemical shift changes are displayed in a surface representation. The surfaces are colored according to electrostatic charge, demonstrating the electrostatic complementarity of the two sites. Side chains for residues that are part of the IgE interaction site are displayed and colored in green. (B) Cartoon representations (top and side views) illustrating the overall architecture of the trimer and the ligand binding sites. The two oligomerization sites are colored blue and red, respectively, the IgE interaction site is green, the CD21 binding site is cyan, and the calcium binding site is yellow. The front two molecules of the trimer are semitransparent.

DISCUSSION

The structure of derCD23 and its complexes with IgE and CD21

The NMR structure of derCD23 confirms that it has the topology of a C-type lectin domain, as predicted by sequence homology to other members of this family. NMR spectra revealed an equilibrium between two structures that differ in the hydrophobic packing between two of the structural elements. Structural plasticity has been suggested to confer an advantage in allowing greater diversity of ligand recognition (27). CD23's conformational heterogeneity could potentially play a role in its interactions with ligands. However, IgE, CD21, or calcium binding do not affect the relative proportions of the two conformers, which leads us to conclude that both conformers bind to these ligands equally well. Surprisingly, occupation of only one of the putative calcium-binding sites (Ca^{2+} site 1) could be confirmed. Because Ca^{2+} site 2 is involved in carbohydrate recognition by other CTLDs, this result is in accord with the observation that glycosylation is not required for the binding to either IgE (28) or CD21(D1-2) (6). The results also demonstrate that calcium is not required to stabilize the configuration of CD23 for binding these ligands.

We have observed cooperativity and biphasicity in the binding of Cε2-4 to derCD23 (Fig. 1 D) and of exCD23 to Cε2-4 (Fig. 1 F). The latter corresponds well with the reported biphasic kinetics of IgE binding to monomers and trimers of membrane CD23 at the cell surface (11, 29). At the concentrations of the Biacore experiments (see Materials and methods), we know from sedimentation equilibrium that both derCD23 and exCD23 are entirely monomeric, and, thus, the IgE Fc must stabilize their oligomerization, more so for exCD23 because it contains the stalk as well as the lectin domain. Ligand-induced oligomerization of exCD23 may be a further example of coupled folding and protein binding (30). In contrast to the interaction with IgE, there was no concentration dependence or evidence of cooperativity in the binding of CD21(D1-2) to derCD23 (Fig. 1, A and C), suggesting that a single lectin domain of CD23 (with a com-

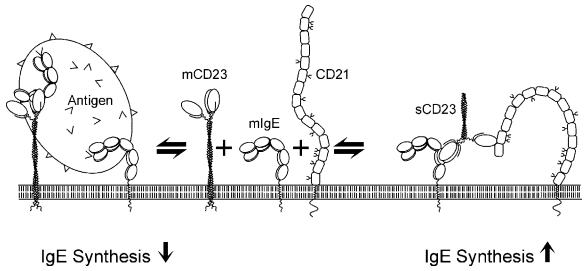

Figure 6. Competition between CD23 and CD21 for membrane IgE on the B cell surface. (left) Co-cross-linking of membrane CD23 and membrane IgE by an allergen–IgE complex leads to down-regulation of IgE synthesis. (right) Trimeric soluble CD23 co-cross-linking of membrane IgE and CD21 leads to up-regulation. IgE binding to membrane CD23 also protects the latter against proteolysis and prevents formation of soluble CD23.

plete tail region) contains the complete binding site for this region of CD21.

In addition to showing that the binding sites on CD23 for IgE and CD21 are distinct from each other (Fig. 4 C) and from the trimerization interface (Fig. 5), we also found that derCD23 can bind both ligands simultaneously to form a trimolecular complex. We observed the formation of high molecular mass complexes between Cε2-4 and derCD23 by NMR and have seen a similar result with Cε2-4 and exCD23 by sedimentation equilibrium (unpublished data). These properties help us to understand the functions of CD23, and, in particular, they support a proposed mechanism of IgE homeostasis, illustrated in Fig. 6 and discussed in detail below.

Up-regulation of IgE synthesis

Soluble CD23 is implicated in the up-regulation of IgE synthesis: its attachment to CD21 on peripheral blood B cells before differentiation into IgE-secreting plasma cells enhances IgE synthesis (2). A mechanism for the up-regulation of IgE synthesis was originally suggested by analogy to the process of up-regulation of antibody synthesis in the immune response by C3d fragments of complement component C3. C3d fragments, covalently linked to the antigen, coligate antigen receptor (IgM) and CD21 on naive B cells (31, 32), leading to cell proliferation and antibody synthesis.

We have founds that B cells express membrane IgE and CD21 before differentiation into the IgE-secreting plasma cells (unpublished data). Thus, soluble CD23 may up-regulate IgE synthesis by coligation of membrane IgE and CD21 on these transitional cells, resulting in selective proliferation and, ultimately, higher levels of IgE synthesis (Fig. 6, right). Such a mechanism is supported by our observation that coligation of membrane IgM and CD21 by anti-IgM (acting as a surrogate antigen) and CD23 stimulates B cell proliferation (33). Our discoveries that the binding sites for IgE and CD21 are distinct and that both ligands can bind simultaneously support the co-cross-linking of membrane IgE and CD21 by soluble CD23. If correct, then the inhibition of membrane CD23 cleavage or soluble CD23 binding to either IgE or CD21 offers potential targets for therapy, and the data presented here will provide a structural basis for designing inhibitors.

Feedback regulation of IgE synthesis

Membrane CD23 is associated with the down-regulation of IgE synthesis (Fig. 6, left). CD23-deficient mice exhibit abnormally high serum IgE levels, whereas CD23-overexpressing mice show decreased IgE synthesis and reduced susceptibility to systemic anaphylaxis (34). Cross-linking of membrane CD23 on human B cells by IgE or IgE–antigen complexes or by anti-CD23 antibodies inhibits B cell proliferation and IgE production (35, 36). An anti-CD23 monoclonal antibody has accordingly shown promise for lowering serum IgE levels in clinical trials (16). Moreover, co-cross-linking of CD23 with surface immunoglobulin induces the apoptosis of B cells (37), and, thus, antigen–IgE complexes may regulate the population of the specific IgE antibody–producing B cells.

Our study sheds light on possible mechanisms of feedback regulation of IgE by membrane CD23. The binding of IgE to membrane CD23 prevents cleavage and release of the soluble CD23 fragments that stimulate IgE synthesis. Our finding that IgE Fc cooperatively binds two lectin domains of CD23 and appears to promote oligomerization of exCD23 explains how IgE might stabilize the trimer of membrane CD23 on the cell surface, rendering it less susceptible to proteolysis. The observation of high molecular mass complex formation between IgE Fc and derCD23 indicates how exogenous IgE could be endocytosed and degraded. Furthermore, the co-cross-linking of membrane CD23 and specific antibodies by IgE–antigen complexes may steal the endogenous membrane IgE from CD21, thus antagonizing the positive feedback pathway (Fig. 6).

Pivotal role of CD23 in IgE homeostasis

The main effector function of IgE is thought to be sensitization of mast cells for allergen triggering of an allergic response. This serves as protection against parasite infections, but confers the risk of allergic disease in susceptible individuals. The lower affinity of IgE for CD23 (K_D = $\sim 10^{-7}$–10^{-8} M) than for FcεRI (K_D = $\sim 10^{-10}$–10^{-11} M), collectively with feedback regulation of IgE synthesis by IgE, ensures that the mast cells remain sensitized once excess IgE has been removed. According to the scheme in Fig. 6, soluble CD23, released by B cells on stimulation in the immune response, would initially up-regulate IgE synthesis by coligating membrane IgE and CD21. As IgE concentrations enter the range in which binding to membrane CD23 becomes important, IgE synthesis would be abruptly terminated. This would preclude the accumulation of dangerous levels of IgE. The isotype specificity of this mechanism is explained by the fact the switch between up- and down-regulation pivots around IgE itself (Fig. 6). The structure of CD23 and the trimer model, the location of its binding sites for IgE and

CD21, and the clustering of CD23 caused by IgE Fc lend support to this mechanism and suggest strategies for down-regulation of IgE levels to treat allergic disease.

MATERIALS AND METHODS

Protein expression and purification. derCD23 (P06734) comprises the amino acids Ser156 to Glu298. The human derCD23 construct was subcloned from CD23 cDNA (38) by PCR. Recombinant derCD23 was expressed in the *Escherichia coli* host strain BL21(DE3), extracted from the cell pellets, and refolded by Taylor's procedure (39). Unlabeled and ^{15}N- and ^{13}C-labeled derCD23 were prepared on minimal media or with the addition of [^{13}C]glucose/[^{15}N]H_4Cl to the media. Proteins were purified by hydrophobic interaction chromatography on a phenyl sepharose column (GE Healthcare). Mass spectrometry of these materials was performed on a mass spectrometer (Micromass Platform-II ESI; Waters). Reverse-phase HPLC-purified unlabeled, ^{15}N-labeled, and ^{13}C, ^{15}N–labeled material had masses of 16,143 ± 4, 16,334 ± 3, and 16,995 ± 5 D, respectively, confirming the identity of the material and indicating that isotope incorporation was highly efficient. ExCD23, comprising Asp48 to Ser321, was subcloned from CD23 cDNA, expressed in *E. coli*, extracted, and refolded as described above for derCD23. Recombinant human CD21(D1-2), Cε2-4 (provided by A. Beavil, Kings College London, London, UK), and Cε3 (provided by N. Price, University of Oxford, Oxford, UK) constructs were prepared as described previously (9, 11, 40, 41).

Surface plasmon resonance. All experiments were performed at 25°C on an automated instrument (Biacore 2000; Biacore AB). A specific binding surface was prepared by coupling derCD23 to a CM5 sensor chip through the amine coupling procedure. Coupling densities of 3,000 (high density) and 400 resonance units (low density) were used. Cε2-4 and CD21(D1-2) in HBS (10 mM Hepes, pH 7.4, 150 mM NaCl, 4 mM $CaCl_2$, and 0.005% [vol/vol] surfactant p20) were injected over the sensor chip at 10 μl min^{-1} with a 3-min association phase followed by a 15-min dissociation phase. Binding was also tested at higher flow rates and showed no change in interaction characteristics. In the reverse binding experiment, a biotinylated Cε2-4 protein was immobilized at low density on a streptavidin chip, and soluble derCD23 or exCD23 was injected over the surface. Biotinylation of Cε2-4 was performed by mixing Cε2-4 with 6-(biotinamidocaproylamido) caproic acid succinamide ester (Sigma-Aldrich) at a ratio of 3:1, a process that generally ensures a single biotinylation site per protein, followed by gel filtration. When necessary, regeneration of the sensor surface was performed using three 60-s pulses of 0.2 M glycine-HCl, pH 2.5. Injections over underivatized sensor surfaces were performed to test for nonspecific binding. The IgE, CD23, and CD21 proteins were well behaved in the Biacore experiments, with essentially no nonspecific binding to control flow cells, efficient regeneration of sensor surfaces, and excellent reproducibility. Standard double referencing data subtraction methods (42) were used before analysis of rates and equilibrium binding. Curve fitting and other data analyses were performed using MicroCal Origin 6.1 (OriginLab Corporation).

NMR spectroscopy. NMR samples were prepared from concentrated derCD23 dialysed into a buffer containing 25 mM Tris, 125 mM NaCl, and 4 mM $CaCl_2$, pH 6.8, and placed in a Shigemi NMR tube (Shigemi Corp.). All NMR data were collected at 35°C on home-built spectrometers operating at proton frequencies of 500, 600, and 750 MHz (Omega/GE Healthcare). The assignment and structure determination of derCD23 were performed using standard heteronuclear NMR experiments as described in McDonnell et al. (43). Assignments made use of the following NMR experiments: HNCA, HN(CO)CA, HNCACB, HN(CO)CACB, HNCO, HN(CA)CO, ^{15}N–TOCSY–HSQC (mixing times of 16 and 25 ms), and HCCH-TOCSY (mixing time of 11 ms). All triple resonance experiments were collected using trosy-based sequences (20). Three residues in the NH_2 or COOH termini (residues 156–157 and 293) and five residues (residues 252–256) in a central loop were not assigned, as well as five other residues in loops and turns (residues 181, 215–216, 249, 263). Several approaches were used to try to help in the assignment of these residues, including changes in temperature, concentration, pH, ionic strength, and $CaCl_2$ concentration, without success. NOE correlations were measured using ^{15}N- and ^{13}C-edited 3D-NOESY experiments and a 2D-NOESY in D_2O (all mixing times of 125 ms). The backbone torsion angles ϕ and ψ were derived for the well-defined secondary structure elements using TALOS (21). Structure calculations were performed using the program CNS (version 1.1) (44) in an ab initio–simulated annealing protocol with a two-stage torsion angle dynamics and a Cartesian dynamics protocol. From 100 calculations, the 20 structures with the lowest energies were selected and subjected to a four-step refinement stage, adjusting for uncertainties in NOE restraints length because of overlap or spectral artifacts. Statistics for the resulting family of structures are listed in Table I.

Backbone ^{15}N relaxation parameters, measuring the rates of ^{15}N longitudinal (R1) and transverse (R2) relaxation and the ^{1}H-^{15}N steady-state NOE, were collected using previously described methods (45). The "model-free" characteristics of the local motions (46) were derived from these parameters using the program DYNAMICS, and hydrodynamic characteristics were calculated using the program ROTDIF (47). Fitting the relaxation rate for all structured residues ($S^2 > 0.8$), the following values for overall rotation were calculated: $\tau_c = 9.32 \pm 0.22$ ns and $D_{||}/D_{\perp} = 1.40 \pm 0.06$.

For chemical shift perturbation experiments, unlabeled ligands were titrated in small aliquots to samples of ^{15}N-labeled derCD23. Chemical shift changes (Δδ) in ^{1}H-^{15}N–HSQC spectra were followed until saturation, typically collecting 6–8 spectra per titration. Where possible, ligand samples were lyophilized and added as a powder to minimize volume changes during the experiment. For the calcium titration, the dissociation constant (K_D) was estimated from the titration curves of all residues that showed considerable chemical shift changes by plotting the relative magnitude of Δδ as a function of calcium concentration. A complete table of chemical shifts for derCD23 at low and high concentrations, chemical shifts for derCD23 bound to CD21, and the chemical shifts during the IgE Cε3 and calcium titrations are available from the BioMagResBank database under accession nos. 6732, 6733, 6734, and 6735.

Fast-exchanging amide protons were determined using a two-dimensional heteronuclear water exchange filter sequence (WEX II-FHSQC) (48). Mixing times of 100 and 500 ms for the water magnetization transfer were set. In the analysis of these data the intensities of the observed peaks were normalized against a native HSQC and plotted against residue number.

Measurements of translational diffusion coefficients were performed using pulsed field gradient methods. 16 1-D spectra, with gradient strengths varying from 6.5 to 65 G cm^{-1}, were acquired. Intensities of NMR signals were fitted to standard equations to derive diffusion coefficients (26).

Online supplemental material. Fig. S1 shows a summary of the derCD23 secondary structure and dynamics analysis. Online supplemental material is available at http://www.jem.org/cgi/content/full/jem.20050811/DC1.

We thank Dr. Andrew Beavil for the gift of Cε2-4 and Naomi Price for Cε3.

J.M. McDonnell, B.J. Sutton, and H.J. Gould acknowledge grant support from the Wellcome Trust, the Medical Research Council (UK), and Asthma UK. R.G. Hibbert was supported by a Wellcome Prize Studentship.

The authors have no conflicting financial interests.

Submitted: 22 April 2005
Accepted: 1 August 2005

REFERENCES

1. Gould, H.J., R.L. Beavil, R. Reljic, J. Shi, C.W. Ma, B.J. Sutton, and R. Ghirlando. 1997. IgE homeostasis: is CD23 the safety switch? *In* IgE Regulation: Molecular Mechanisms. D. Vercelli, editor. John Wiley & Sons Inc., New York. 35–59.
2. Aubry, J.P., S. Pochon, P. Graber, K.U. Jansen, and J.Y. Bonnefoy. 1992. CD21 is a ligand for CD23 and regulates IgE production. *Nature*. 358:505–507.

3. Soilleux, E.J., R. Barten, and J. Trowsdale. 2000. DC-SIGN; a related gene, DC-SIGNR; and CD23 form a cluster on 19p13. *J. Immunol.* 165:2937–2942.
4. Mossalayi, M.D., M. Arock, G. Delespesse, H. Hofstetter, B. Bettler, A.H. Dalloul, E. Kilchherr, F. Quaaz, P. Debre, and M. Sarfati. 1992. Cytokine effects of CD23 are mediated by an epitope distinct from the IgE binding site. *EMBO J.* 11:4323–4328.
5. Shi, J., R. Ghirlando, R.L. Beavil, A.J. Beavil, M.B. Keown, R.J. Young, R.J. Owens, B.J. Sutton, and H.J. Gould. 1997. Interaction of the low-affinity receptor CD23/Fc epsilonRII lectin domain with the Fc epsilon3-4 fragment of human immunoglobulin E. *Biochemistry.* 36: 2112–2122.
6. Aubry, J.P., S. Pochon, J.F. Gauchat, A. Nueda-Marin, V.M. Holers, P. Graber, C. Siegfried, and J.Y. Bonnefoy. 1994. CD23 interacts with a new functional extracytoplasmic domain involving N-linked oligosaccharides on CD21. *J. Immunol.* 152:5806–5813.
7. Wan, T., R.L. Beavil, S.M. Fabiane, A.J. Beavil, M.K. Sohi, M. Keown, R.J. Young, A.J. Henry, R.J. Owens, H.J. Gould, and B.J. Sutton. 2002. The crystal structure of IgE Fc reveals an asymmetrically bent conformation. *Nat. Immunol.* 3:681–686.
8. Wurzburg, B.A., S.C. Garman, and T.S. Jardetzky. 2000. Structure of the human IgE-Fc C epsilon 3-C epsilon 4 reveals conformational flexibility in the antibody effector domains. *Immunity.* 13:375–385.
9. Szakonyi, G., J.M. Guthridge, D. Li, K. Young, V.M. Holers, and X.S. Chen. 2001. Structure of complement receptor 2 in complex with its C3d ligand. *Science.* 292:1725–1728.
10. Padlan, E.A., and B.A. Helm. 1993. Modeling of the lectin-homology domains of the human and murine low-affinity Fc epsilon receptor (Fc epsilon RII/CD23). *Receptor.* 3:325–341.
11. Beavil, R.L., P. Graber, N. Aubonney, J.Y. Bonnefoy, and H.J. Gould. 1995. CD23/Fc epsilon RII and its soluble fragments can form oligomers on the cell surface and in solution. *Immunology.* 84:202–206.
12. Letellier, M., M. Sarfati, and G. Delespesse. 1989. Mechanisms of formation of IgE-binding factors (soluble CD23)–I. Fc epsilon R II bearing B cells generate IgE-binding factors of different molecular weights. *Mol. Immunol.* 26:1105–1112.
13. Schulz, O., B.J. Sutton, R.L. Beavil, J. Shi, H.F. Sewell, H.J. Gould, P. Laing, and F. Shakib. 1997. Cleavage of the low-affinity receptor for human IgE (CD23) by a mite cysteine protease: nature of the cleaved fragment in relation to the structure and function of CD23. *Eur. J. Immunol.* 27:584–588.
14. Gould, H.J., B.J. Sutton, A.J. Beavil, R.L. Beavil, N. McCloskey, H.A. Coker, D. Fear, and L. Smurthwaite. 2003. The biology of IgE and the basis of allergic disease. *Annu. Rev. Immunol.* 21:579–628.
15. Plater-Zyberk, C., and J.Y. Bonnefoy. 1995. Marked amelioration of established collagen-induced arthritis by treatment with antibodies to CD23 in vivo. *Nat. Med.* 1:781–785.
16. Rosenwasser, L.J., W.W. Busse, R.G. Lizambri, T.A. Olejnik, and M.C. Totoritis. 2003. Allergic asthma and an anti-CD23 mAb (IDEC-152): results of a phase I, single-dose, dose-escalating clinical trial. *J. Allergy Clin. Immunol.* 112:563–570.
17. Mavromatis, B.H., and B.D. Cheson. 2004. Novel therapies for chronic lymphocytic leukemia. *Blood Rev.* 18:137–148.
18. Richards, M.L., and D.H. Katz. 1990. The binding of IgE to murine Fc epsilon RII is calcium-dependent but not inhibited by carbohydrate. *J. Immunol.* 144:2638–2646.
19. Pochon, S., P. Graber, M. Yeager, K. Jansen, A.R. Bernard, J.P. Aubry, and J.Y. Bonnefoy. 1992. Demonstration of a second ligand for the low affinity receptor for immunoglobulin E (CD23) using recombinant CD23 reconstituted into fluorescent liposomes. *J. Exp. Med.* 176:389–397.
20. Pervushin, K., R. Riek, G. Wider, and K. Wuthrich. 1997. Attenuated T2 relaxation by mutual cancellation of dipole-dipole coupling and chemical shift anisotropy indicates an avenue to NMR structures of very large biological macromolecules in solution. *Proc. Natl. Acad. Sci. USA.* 94:12366–12371.
21. Cornilescu, G., F. Delaglio, and A. Bax. 1999. Protein backbone angle restraints from searching a database for chemical shift and sequence homology. *J. Biomol. NMR.* 13:289–302.
22. Zelensky, A.N., and J.E. Gready. 2003. Comparative analysis of structural properties of the C-type-lectin-like domain (CTLD). *Proteins.* 52: 466–477.
23. Taylor, M.E., and K. Drickamer. 2003. Structure-function analysis of C-type animal lectins. *Methods Enzymol.* 363:3–16.
24. East, L., S. Rushton, M.E. Taylor, and C.M. Isacke. 2002. Characterization of sugar binding by the mannose receptor family member, Endo180. *J. Biol. Chem.* 277:50469–50475.
25. Nissim, A., S. Schwarzbaum, R. Siraganian, and Z. Eshhar. 1993. Fine specificity of the IgE interaction with the low and high affinity Fc receptor. *J. Immunol.* 150:1365–1374.
26. Altieri, A., D. Hinton, and R. Byrd. 1995. Association of biomolecular systems via pulsed field gradient NMR self-diffusion measurements. *J. Am. Chem. Soc.* 117:7566–7567.
27. Yin, J., A.E. Beuscher IV, S.E. Andryski, R.C. Stevens, and P.G. Schultz. 2003. Structural plasticity and the evolution of antibody affinity and specificity. *J. Mol. Biol.* 330:651–656.
28. Vercelli, D., B. Helm, P. Marsh, E. Padlan, R.S. Geha, and H. Gould. 1989. The B-cell binding site on human immunoglobulin E. *Nature.* 338:649–651.
29. Dierks, S.E., W.C. Bartlett, R.L. Edmeades, H.J. Gould, M. Rao, and D.H. Conrad. 1993. The oligomeric nature of the murine Fc epsilon RII/CD23. Implications for function. *J. Immunol.* 150:2372–2382.
30. Dyson, H.J., and P.E. Wright. 2002. Coupling of folding and binding for unstructured proteins. *Curr. Opin. Struct. Biol.* 12:54–60.
31. Carter, R.H., and D.T. Fearon. 1992. CD19: lowering the threshold for antigen receptor stimulation of B lymphocytes. *Science.* 256:105–107.
32. Dempsey, P.W., and D.T. Fearon. 1996. Complement: instructing the acquired immune system through the CD21/CD19 complex. *Res. Immunol.* 147:71–75 (discussion 119–120).
33. Reljic, R., G. Cosentino, and H.J. Gould. 1997. Function of CD23 in the response of human B cells to antigen. *Eur. J. Immunol.* 27:572–575.
34. Payet, M., and D.H. Conrad. 1999. IgE regulation in CD23 knockout and transgenic mice. *Allergy.* 54:1125–1129.
35. Luo, H.Y., H. Hofstetter, J. Banchereau, and G. Delespesse. 1991. Cross-linking of CD23 antigen by its natural ligand (IgE) or by anti-CD23 antibody prevents B lymphocyte proliferation and differentiation. *J. Immunol.* 146:2122–2129.
36. Sherr, E., E. Macy, H. Kimata, M. Gilly, and A. Saxon. 1989. Binding the low affinity Fc epsilon R on B cells suppresses ongoing human IgE synthesis. *J. Immunol.* 142:481–489.
37. Campbell, K.A., E.J. Studer, M.A. Kilmon, A. Lees, F. Finkelman, and D.H. Conrad. 1997. Induction of B cell apoptosis by co-cross-linking CD23 and sIg involves aberrant regulation of c-myc and is inhibited by bcl-2. *Int. Immunol.* 9:1131–1140.
38. Ikuta, K., M. Takami, C.W. Kim, T. Honjo, T. Miyoshi, Y. Tagaya, T. Kawabe, and J. Yodoi. 1987. Human lymphocyte Fc receptor for IgE: sequence homology of its cloned cDNA with animal lectins. *Proc. Natl. Acad. Sci. USA.* 84:819–823.
39. Taylor, M.A., K.A. Pratt, D.F. Revell, K.C. Baker, I.G. Sumner, and P.W. Goodenough. 1992. Active papain renatured and processed from insoluble recombinant propapain expressed in *Escherichia coli*. *Protein Eng.* 5:455–459.
40. Henry, A.J., J.M. McDonnell, R. Ghirlando, B.J. Sutton, and H.J. Gould. 2000. Conformation of the isolated cepsilon3 domain of IgE and its complex with the high-affinity receptor, FcepsilonRI. *Biochemistry.* 39:7406–7413.
41. Young, R.J., R.J. Owens, G.A. Mackay, C.M. Chan, J. Shi, M. Hide, D.M. Francis, A.J. Henry, B.J. Sutton, and H.J. Gould. 1995. Secretion of recombinant human IgE-Fc by mammalian cells and biological activity of glycosylation site mutants. *Protein Eng.* 8:193–199.
42. Myszka, D.G. 1999. Improving biosensor analysis. *J. Mol. Recognit.* 12: 279–284.
43. McDonnell, J.M., R. Calvert, R.L. Beavil, A.J. Beavil, A.J. Henry, B.J. Sutton, H.J. Gould, and D. Cowburn. 2001. The structure of the IgE Cepsilon2 domain and its role in stabilizing the complex with its high-affinity receptor FcepsilonRIalpha. *Nat. Struct. Biol.* 8:437–441.
44. Brunger, A.T., P.D. Adams, G.M. Clore, W.L. DeLano, P. Gros,

R.W. Grosse-Kunstleve, J.S. Jiang, J. Kuszewski, M. Nilges, N.S. Pannu, et al. 1998. Crystallography & NMR system: a new software suite for macromolecular structure determination. *Acta Crystallogr. D Biol. Crystallogr.* 54:905–921.

45. McDonnell, J.M., D. Fushman, C.L. Milliman, S.J. Korsmeyer, and D. Cowburn. 1999. Solution structure of the proapoptotic molecule BID: a structural basis for apoptotic agonists and antagonists. *Cell.* 96:625–634.
46. Lipari, G., and A. Szabo. 1982. Model-free approach to the interpretation of nuclear magnetic resonance relaxation in macromolecules. 1. Theory and range of validity. *J. Am. Chem. Soc.* 104:4546–4559.
47. Walker, O., R. Varadan, and D. Fushman. 2004. Efficient and accurate determination of the overall rotational diffusion tensor of a molecule from (15)N relaxation data using computer program ROTDIF. *J. Magn. Reson.* 168:336–345.
48. Mori, S., C. Abeygunawardana, P.C. van Zijl, and J.M. Berg. 1996. Water exchange filter with improved sensitivity (WEX II) to study solvent-exchangeable protons. Application to the consensus zinc finger peptide CP-1. *J. Magn. Reson. B.* 110:96–101.